RESEARCH ARTICLE

Open Access

CrossMark

Simultaneous measurements of elastic wave velocities and electrical conductivity in a brine-saturated granitic rock under confining pressures and their implication for interpretation of geophysical observations

Tohru Watanabe[1*] and Akiyoshi Higuchi[1,2]

Abstract

Simultaneous measurements of elastic wave velocity and electrical conductivity in a brine-saturated granitic rock were conducted under confining pressures of up to 180 MPa. Contrasting changes in velocity and conductivity were observed. As the confining pressure increased to 50 MPa, compressional and shear wave velocities increased by less than 10 %. On the other hand, electrical conductivity decreased by an order of magnitude. Both changes must be caused by the closure of cracks under pressures. Microstructural examinations showed that most cracks were open grain boundaries. In reality, a crack is composed of many segments with different apertures. If crack segments have a similar length, segments with small apertures are closed at low pressures to greatly reduce conductivity, while those with wide apertures are open even at high pressures. The latter must form an interconnected fluid path to maintain the electrical conduction through fluid. A power law distribution of apertures causes a steep decrease in conductivity at low pressures. An empirical relation between the crack density parameter and normalized conductivity was obtained. The normalized conductivity is the ratio of bulk conductivity to the conductivity of a pore fluid. This relation should be a basis for quantitative interpretation of observed seismic velocity and electrical conductivity.

Keywords: Seismic velocity, Electrical conductivity, Fluid, Crack, Pore

Background

Geophysical mapping of fluids is critical for understanding geodynamic processes including seismic activities. Fluids can significantly reduce the frictional strength of fault zones (e.g., Sibson 2009) and weaken the flow strength of rocks through fluid-assisted processes such as pressure solution (e.g., Rutter 1983). Seismic velocity and electrical resistivity structures have been constructed to study the fluid distribution in the continental crust. Though a lot of studies have suggested the pervasive existence of aqueous fluids in the crust (e.g., Ogawa et al. 2001), the fluid distribution has not been quantitatively constrained.

Observations on seismic velocity and electrical resistivity should be combined to make a quantitative inference on fluid distribution. It is impossible to infer the amount of fluid only from observed seismic velocity. Seismic velocity of a fluid-bearing rock depends on the elastic properties of the solid and fluid phases and the geometry and amount of the fluid (e.g., Takei 2002). Even if we know the elastic property and geometry of the fluid, we cannot estimate the amount of fluid. Since the lithology of a study region is usually unknown, elastic properties of the rock matrix must be assumed. In

* Correspondence: twatnabe@sci.u-toyama.ac.jp
[1]Graduate School of Science and Engineering, University of Toyama, 3190 Gofuku, Toyama 930-8555, Japan
Full list of author information is available at the end of the article

Springer

addition, the fluid amount cannot be inferred only from observed resistivity. Electrical resistivity of a fluid-bearing rock depends on the resistivity of solid and fluid phases and the geometry and amount of fluid (e.g., Schmeling 1986). The resistivity of fluid is usually much lower than that of the rock matrix. If the fluid phase forms an interconnected path, the electrical conduction is dominated by the conduction through the fluid phase. The bulk conductivity hardly depends on the conductivity of the rock matrix. The estimation of the amount of fluid requires the knowledge of fluid resistivity, which is usually unknown. Owing to the uncertainty in fluid resistivity, the estimated amount of fluid must thus have large uncertainty. However, the fluid amount estimated from observed resistivity must be identical to that estimated from observed seismic velocity. This can be a constraint to reduce uncertainty in the interpretation of velocity and resistivity.

In order to make a combined interpretation of velocity and resistivity, we must have a thorough understanding of velocity and resistivity in fluid-bearing rocks. Velocity and resistivity in a fluid-bearing rock should be formulated as a function of a structural parameter such as fluid volume fraction. Fluids are mainly situated within cracks in crustal rocks (e.g., O'Connell and Budiansky 1974). Based on the inclusion theory (Eshelby 1957), the influence of fluid-filled cracks on elastic properties of rocks has long been studied. For thin cracks, the effective elastic constants are formulated as a function of the crack density parameter (O'Connell and Budiansky 1974). In their pioneering work, Brace et al. (1965) showed that electrical resistivity of brine-saturated rocks largely increased with increasing confining pressure. The increase in confining pressure closed cracks to squeeze brine out to result in a large increase in resistivity. Later, the observed resistivity change was reasonably reproduced by a percolation model (Johnson and Manning 1986). If we relate the change in resistivity to that in velocity, we can make a combined interpretation of velocity and resistivity. Simultaneous measurements of velocity and resistivity in a fluid-bearing rock are required to give a basis for the combined interpretation.

We have conducted simultaneous measurements of elastic wave velocity and electrical conductivity (the inverse of resistivity) of a brine-saturated granitic rock with changing confining and pore-fluid pressures. In this paper, we report measurements of velocity and conductivity and examined pore spaces. The nature of the conduction path will be discussed with the percolation model devised by Johnson and Manning (1986). Based on the empirical relation between electrical conductivity and crack density parameter, we propose a method for the combined interpretation of seismic velocity and electrical resistivity.

Methods

Samples

A fine-grained (100–500 μm) biotite granite (Aji, Kagawa prefecture, Japan) was used as a rock sample. The rock sample is composed of 52.8 % plagioclase, 36.0 % quartz, 3.0 % K-feldspar, and 8.2 % biotite (Fig. 1a). The apparent density is 2.658–2.668 g/cm^3, and the porosity is 1.9–2.3 % (Table 1). Each sample has a cylindrical shape with dimensions of 26 mm in diameter and 30 mm in length. The apparent density was calculated from the apparent volume and the mass of a cylindrical sample. The porosity was calculated from the apparent density and the density of the solid matrix. The density of the solid matrix was calculated from the volume and mass of a crushed rock sample. The volume was measured with the gas expansion method.

Pores in a rock sample (AJG02) were examined with scanning electron microscopy (SEM) and X-ray computer-aided tomography (CT). An SEM image (Fig. 1b) shows that there are two types of cracks: intra-grain cracks (igc) and grain boundary cracks (open grain boundaries, ogb). Numerous round pores are seen on the polished surface. However, in addition to real pores, they include damages from polishing. X-ray CT images (Fig. 1c, d) show that open grain boundaries (arrows) are pervasive in a rock sample and that there are also a number of round pores (rp), which might be traces of fluids and do not seem to form an interconnected path of fluid. X-ray CT observation was conducted by using a CT system (v|tome|x L300, GE Sensing & Inspection Technologies) at Tokyo Metropolitan Industrial Technology Research Institute, Jonan Branch. A sample for X-ray CT (D = 2 mm, L = 6 mm) was made from Sample AJG02 with ultrasonic machining.

Ultrasonic velocity and strain measurements on dry samples

Ultrasonic velocities were measured in a dry rock sample (AJG02) to study the anisotropy in elasticity of rock samples. Velocity measurements were made in the axial direction and two mutually orthogonal radial directions of the cylindrical sample. One compressional wave velocity and two shear wave velocities were measured in each of three orthogonal directions. Two shear waves propagating in one direction oscillate in mutually orthogonal directions. Measurements were conducted at room temperature and confining pressures of up to 177 MPa with a pressure vessel (Riken, PV-2 M-S6F). Silicone oil (Shin-Etsu Chemical, KF-96-100cs) was used as a pressure medium.

The pulse transmission technique was employed by using Pb(Zr,Ti)O$_3$ transducers with the resonant frequency of 2 MHz. The method was similar to that described in Watanabe et al. (2011). Transducers were
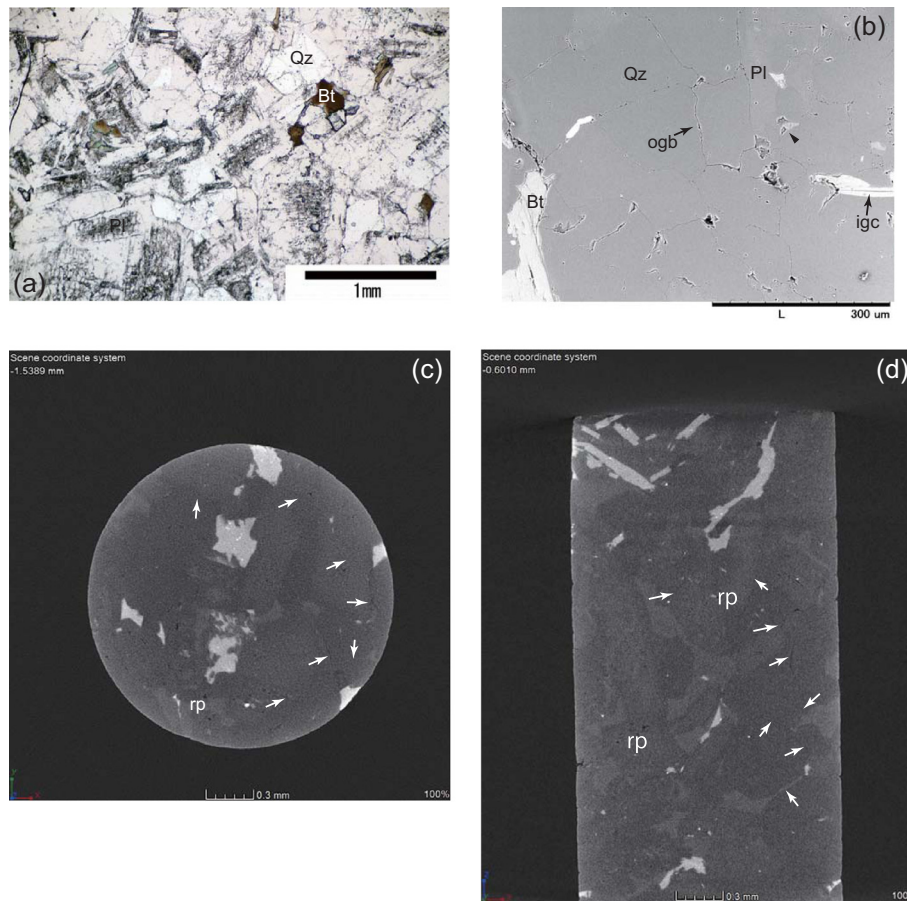
Fig. 1 Microstructures of a granitic rock sample (AJG02). *Pl* plagioclase, *Qz* quartz, *Bt* biotite. **a** A photomicrograph (plane light). The width is parallel to the axis of the cylindrical rock sample. **b** An SEM image. Both intragrain cracks (igc) and intergrain cracks (ogb) can be seen. A *triangle* shows damage from polishing. **c** Radial and **d** axial cross-sectional images of X-ray CT of a cylindrical sample ($D = 2$ mm, $L = 6$ mm), the axis of which is perpendicular to the thin section. Open grain boundaries (*arrows*) seem to be interconnected. Round pores (rp) are seen on grain boundaries and inside grains

glued to the sample, which was covered with RTV rubber (Shin-Etsu Chemical, KE-45). A function generator (Hewlett Packard, 33120A) applied an electrical rectified pulse to one transducer to excite an elastic wave. The other transducer received the transmitted elastic wave and converted it to an electrical signal, which was digitized and averaged over 1024 times by a digital oscilloscope (Agilent Technologies, 54621A). The sampling interval was 20 ns, and the digitized 8-bit signal was

transferred to a computer for analysis. Velocities were calculated from the path length and the travel time.

Linear strains were measured on a dry rock sample (AJG07) under confining pressures to evaluate the volume fraction of cracks. Strains were measured in three mutually orthogonal directions of the cylindrical sample. Measurements were made with a data logger (Tokyo Sokki, TDS-301) and electrical resistance strain gages (Kyowa Electronic Instruments, KFG-1 N-120-C1-11) bonded to the sample surface.

Ultrasonic velocity and electrical conductivity measurements on fluid-saturated samples

Ultrasonic velocity and electrical conductivity were measured on fluid-saturated rock samples at room temperature and confining pressures of up to 125 MPa. The confining and pore-fluid pressures were separately controlled by different pumps (Fig. 2a). A pressure vessel (Riken-Seiki, PV-2 M-S14) was equipped with a plastic
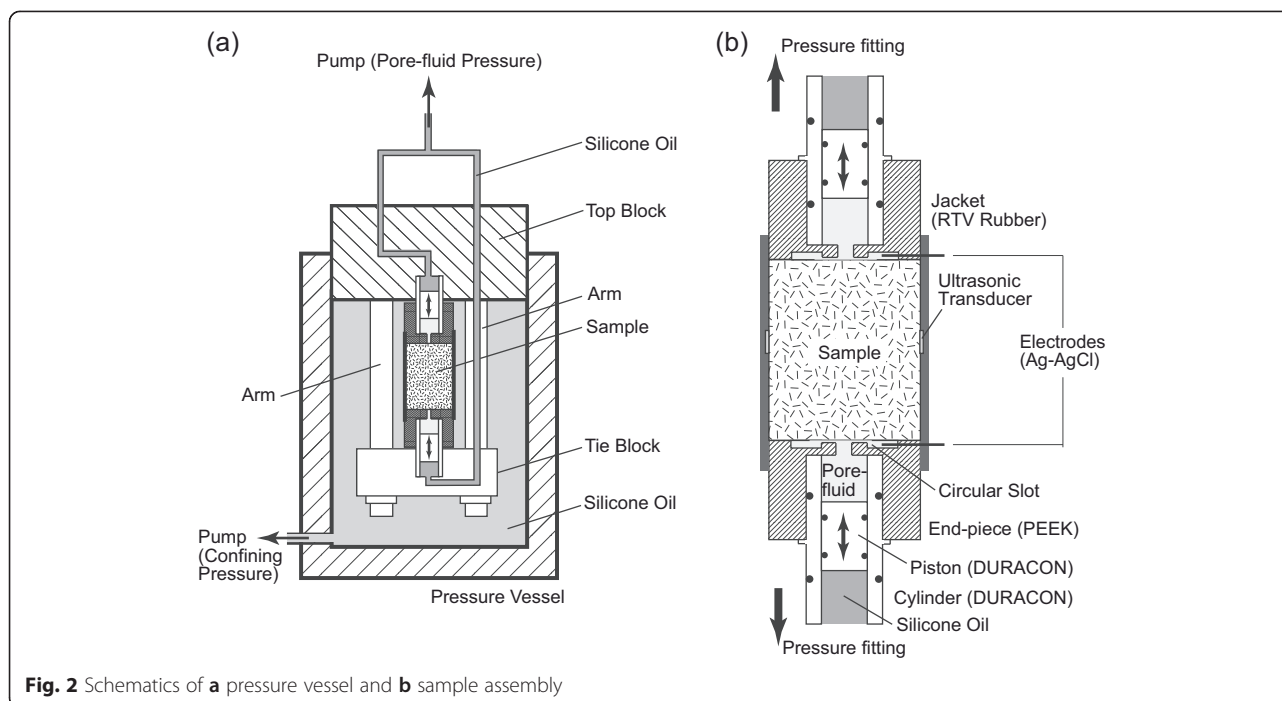
Table 1 List of samples used in this study

Sample	Density (g/cm³)	Porosity (%)	Measurements
AJG02	2.668(2)	1.9(7)	Vp, Vs (dry)
AJG04	2.658(3)	2.3(7)	Vp, Vs, conductivity (wet)
AJG05	2.664(3)	2.1(7)	Vp, conductivity (wet)
AJG07	2.667(2)	2.0(7)	Vp, strain (dry)

The number inside brackets shows the error in the last digit

Fig. 2 Schematics of **a** pressure vessel and **b** sample assembly

piston-cylinder system, which was employed for pore-fluid pressure control and electrical isolation (Watanabe and Higuchi 2014). A pump for controlling pore-fluid pressure moves the piston to change the pore-fluid pressure. The aqueous pore fluid is electrically isolated from the metal work of the pressure vessel.

A sample assembly is shown in Fig. 2b. A cylindrical sample was firstly evacuated and saturated with 0.01 mol/L KCl aqueous solution and assembled with end-pieces. A DURACON (acetal copolymer) piston-cylinder system is inserted in a PEEK end-piece. DURACON and PEEK were selected for their high strength. DURACON can minimize the resistance to the piston movement. RTV rubber was used as a jacketing material. The sample assembly was attached to the top block of the pressure vessel with two arms and a tie block (Fig. 2a). Along with the compression in radial directions, the silicone oil between the top block and the upper end-piece and between the tie block and the lower end-piece compresses a sample in the axial direction, causing a hydrostatic compression. The right arm and the tie block are designed to work as a channel for silicone oil (viscosity ~ 0.1 Pa·s) to move the lower piston. The upper piston is moved by the silicone oil in a channel through the top block.

Compressional and shear wave velocities were measured by the pulse transmission technique. Measurements were made in mutually orthogonal radial directions of the cylindrical sample. The shear wave oscillates parallel to the axis of the sample. $Pb(Zr,Ti)O_3$ transducers with the resonant frequency of 2 MHz were
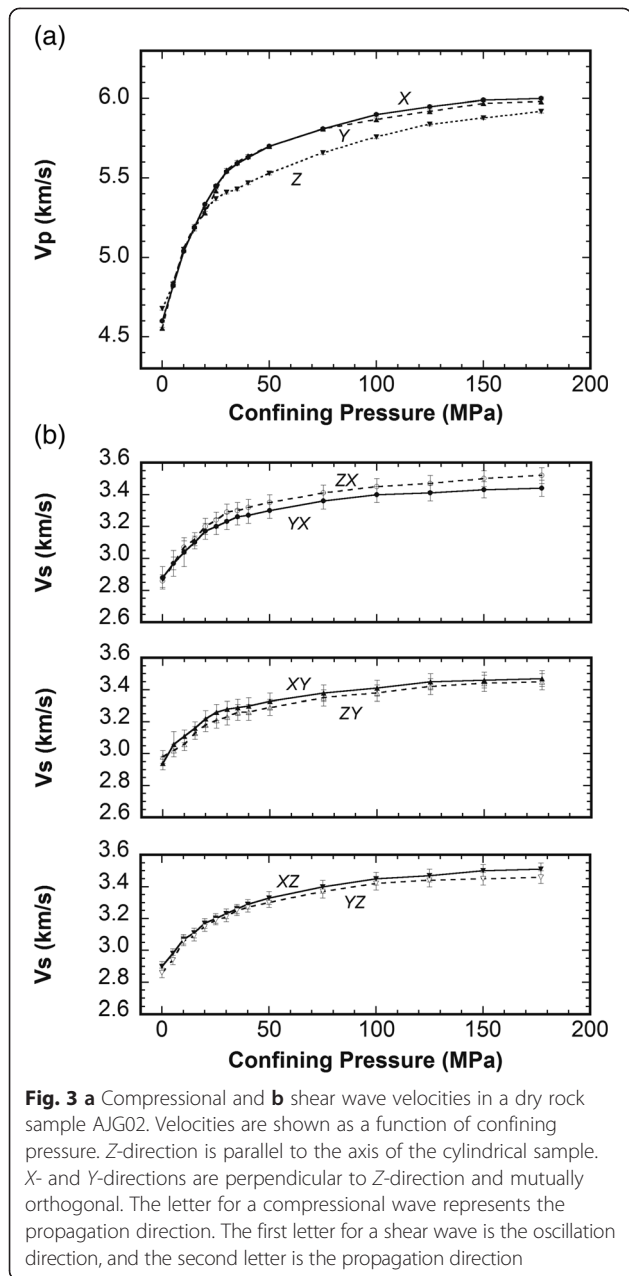
bonded to the sample surface which was coated with an epoxy resin for electrical isolation between the pore fluid and transducers. A function generator (Agilent Technologies, 33220A) and a digital oscilloscope (Agilent Technologies, DSO5012A) were used for pulse excitation and data acquisition, respectively.

Electrical impedance was measured in the axial direction by using an LCR meter (NF, ZM2355) with the two-electrode method. Ag-AgCl electrodes were made as in Watanabe and Katagishi (2006). The PEEK end-piece has a hole and a circular slot on the sample side (Fig. 2b). The pore fluid can flow between the hole and the slot. The frequency range was from 40 Hz to 200 kHz. The conductivity was calculated from the sample resistance, the length, and the cross-sectional area of a sample.

Results

Compressional and shear wave velocities in a dry sample

Compressional and shear wave velocities in a dry sample (AJG02) are shown as a function of confining pressure in Fig. 3. Measurements were made during the increase in confining pressure. The Z-direction was set parallel to the axis of the cylindrical sample. The X- and Y-directions are mutually orthogonal and perpendicular to the cylinder axis. Both compressional and shear wave velocities increase with increasing confining pressure. The increase in velocity is larger for compressional waves (~1.5 km/s) than for shear waves (~0.6 km/s). The increase rate of velocity is greatly reduced at pressures higher than 100 MPa. The increase in velocity must thus be caused by the closure of pores. If we consider a

Fig. 3 a Compressional and **b** shear wave velocities in a dry rock sample AJG02. Velocities are shown as a function of confining pressure. Z-direction is parallel to the axis of the cylindrical sample. X- and Y-directions are perpendicular to Z-direction and mutually orthogonal. The letter for a compressional wave represents the propagation direction. The first letter for a shear wave is the oscillation direction, and the second letter is the propagation direction

spheroidal pore with aspect ratio $\alpha = c/a$, where a and c are the lengths of the semi- major and minor axes, the closure pressure is given by

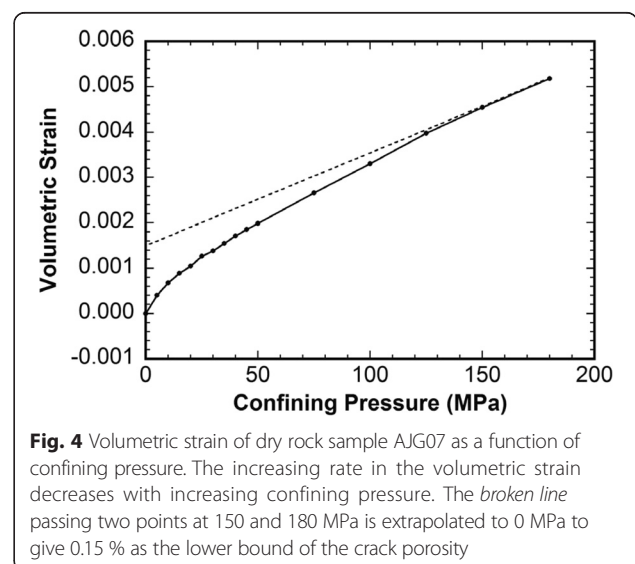$$p_c = \frac{\pi E \alpha}{4(1 - \nu^2)}, \qquad (1)$$

where E and ν are Young's modulus and Poisson's ratio, respectively (Walsh 1965). Pores with smaller aspect ratios thus close at lower pressures.

The sample shows weak velocity anisotropy in the whole range of confining pressure. The anisotropy in compressional and shear wave velocities is quite weak at

177 MPa. The difference between the fastest and slowest compressional wave velocities is only 1.3 %, and no significant difference in shear wave velocity can be seen between two oscillation directions (Fig. 3b). Since the influence of pores is sufficiently suppressed, the elastic wave velocities at 177 MPa are mainly governed by elastic properties of the solid matrix. The solid matrix is thus almost isotropic in elasticity. Although spheroidal pores with large aspect ratios could still be open, their influence on elastic properties is sufficiently small. Elastic wave velocities at atmospheric pressure, which are strongly affected by oblate spheroidal pores, also show weak anisotropy. In consideration of the weak anisotropy in elasticity of the solid matrix, the oblate spheroidal pores, which we call cracks hereafter, must thus be almost randomly oriented.

Volumetric strain in a dry sample

Volumetric strain in a dry rock sample (AJG07) is shown in Fig. 4 as a function of confining pressure. Measurements were made during the increase in confining pressure. The volumetric strain takes positive values for contraction. Linear strains in three mutually orthogonal directions showed that the rock sample deformed isotropically under hydrostatic conditions. The volumetric strain is given by the sum of the three strains. The magnitude of the volumetric strain increases and its increasing rate decreases with increasing confining pressure. The nonlinear increase with pressure is attributed to the closure of cracks. When all cracks are closed, the volumetric strain is caused by the elastic deformation of the solid matrix, and it increases linearly with pressure. The extrapolation of the linear trend to 0 MPa provides an estimate of the crack porosity (e.g., Walsh 1965). However, a linear trend due to elastic deformation of the

Fig. 4 Volumetric strain of dry rock sample AJG07 as a function of confining pressure. The increasing rate in the volumetric strain decreases with increasing confining pressure. The *broken line* passing two points at 150 and 180 MPa is extrapolated to 0 MPa to give 0.15 % as the lower bound of the crack porosity

solid matrix was not observed in our experiment, since the confining pressure is less than 200 MPa. A line passing two points at 150 and 180 MPa provides an estimate of the crack porosity, which is 0.15 % as the intercept on the volumetric strain axis. It is the lower bound of the crack porosity, since the linear trend due to elastic deformation of the solid matrix has a more gradual slope.

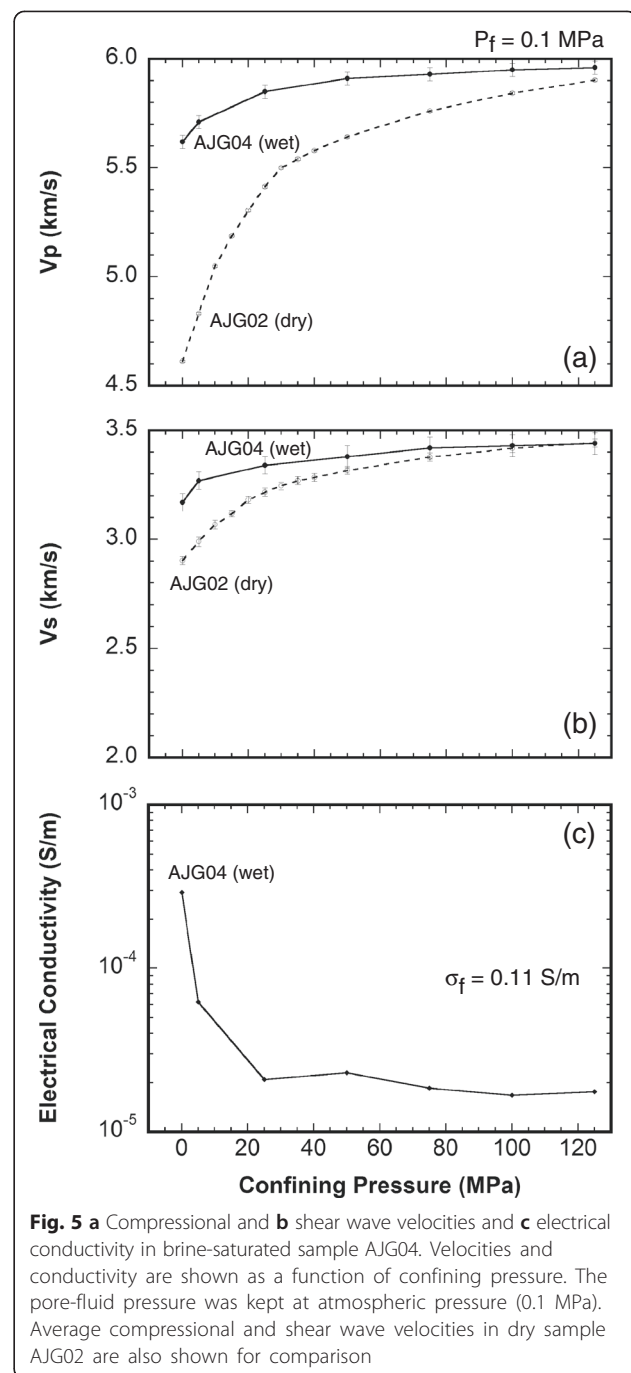### Influence of confining pressure on velocities and conductivity

Simultaneous measurements of velocities and conductivity were made on wet sample AJG04 at confining pressures of up to 125 MPa. The pore-fluid pressure was kept at 0.1 MPa (atmospheric pressure). Compressional and shear wave velocities and electrical conductivity are shown in Fig. 5 as a function of confining pressure. Average compressional and shear wave velocities in dry sample AJG02 are shown for comparison. The confining pressure was first increased to 5 MPa and then increased to 25, 50, 75, 100, and 125 MPa. Velocities and conductivity were allowed to become stationary values before changing the confining pressure. Each pressure condition was kept for 50–100 h. Measurements were made during the increase in confining pressure.

Velocities increased but conductivity decreased with increasing confining pressure. Most changes were observed at confining pressures lower than 50 MPa. The velocities in AJG04 (wet) were higher than those in AJG02 (dry), but the difference between velocities in wet and dry samples decreased with increasing pressure. The changes in velocities and conductivity must thus be attributed to the closure of pores with increasing pressure. The compressional wave velocity increased by 0.34 km/s (6.0 %) from 0.1 to 125 MPa and the shear wave velocity by 0.27 km/s (8.5 %).
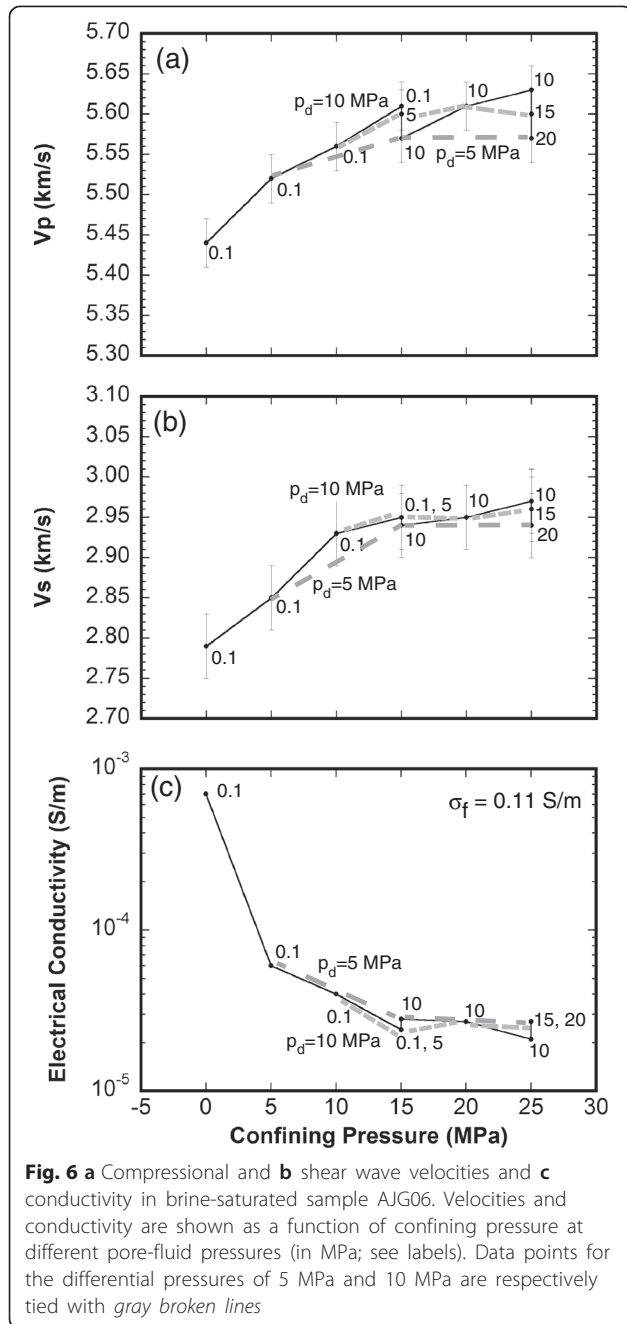
Conductivity showed a large change at low pressures in contrast to velocity changes. Conductivity decreased by more than one order of magnitude from 0.1 to 25 MPa but showed no remarkable change at higher pressures. Similar changes in conductivity have been observed in previous studies (Brace et al. 1965; Lockner and Byerlee 1985). Though the porosity was quite low, the observed conductivity clearly demonstrated the interconnection of fluid. The change in conductivity suggests that the connectivity was greatly reduced by the closure of pores.

Influence of pore-fluid pressure on velocities and conductivity

Velocity and conductivity in wet sample AJG06 were measured at various confining and pore-fluid pressures. Compressional and shear wave velocities and electrical conductivity are shown in Fig. 6 as a

Fig. 5 a Compressional and **b** shear wave velocities and **c** electrical conductivity in brine-saturated sample AJG04. Velocities and conductivity are shown as a function of confining pressure. The pore-fluid pressure was kept at atmospheric pressure (0.1 MPa). Average compressional and shear wave velocities in dry sample AJG02 are also shown for comparison

function of confining and pore-fluid pressures. The confining pressure was first increased to 5, 10, and 15 MPa, while the pore-fluid pressure was kept at 0.1 MPa. The confining pressure was then kept at 15 MPa, and the pore-fluid pressure was increased to 5 and 10 MPa. The confining and pore-fluid pressures were then increased alternately. Each pressure condition was kept for 50–100 h until velocities and conductivity become stationary values. The differential pressure, which is given by

Fig. 6 a Compressional and **b** shear wave velocities and **c** conductivity in brine-saturated sample AJG06. Velocities and conductivity are shown as a function of confining pressure at different pore-fluid pressures (in MPa; see labels). Data points for the differential pressures of 5 MPa and 10 MPa are respectively tied with *gray broken lines*

$$p_d = p_c - p_f,$$

is also indicated in Fig. 6.

The pore-fluid pressure and confining pressure have influences on velocities and conductivity in the opposite directions. When the confining pressure was kept constant, velocities decreased but conductivity increased with increasing pore-fluid pressure. The increase in pore-fluid pressure must open pores to decrease velocities and increase conductivity.

Neither velocities nor conductivity was constant at constant differential pressures. Velocities increased but conductivity decreased at a constant differential pressure as the confining pressure was increased. Similar changes in velocity were reported for oceanic basalt and dolerite (Christensen 1984) and Berea sandstone (Christensen and Wang 1985). When confining pressure is increased, the pore-fluid pressure must be increased by an amount greater than the confining pressure to maintain a constant velocity. The theory of fluid-saturated porous materials (Biot and Willis 1957; Geertsma 1957) showed that the bulk volumetric deformation is not governed by the differential pressure but by the effective pressure

$$p_{\mathrm{eff}} = p_c - n p_f$$

$$n = 1 - \frac{\beta_s}{\beta},$$

where β_s and β are the compressibility of the solid grain and bulk material, respectively. Christensen and Wang (1985) suggested that a physical property sensitive to bulk volume shows a similar effective pressure law. Both velocity and conductivity are strongly dependent on the confining pressure of less than 50 MPa. They are sensitive to bulk volume and thus expected to depend on the effective pressure. The compressibility of a bulk sample is evaluated to be 4.4×10^{-11} (1/Pa) at the confining pressure of 10 MPa from the volumetric strain of a dry sample (Fig. 4). The compressibility of a plagioclase grain, which is the dominant phase, is 2.0×10^{-11} (1/Pa) (Hearmon 1979). These compressibility values give $n = 0.55$. When confining pressure is increased by Δp, the pore-fluid pressure must be increased by $1.8 \Delta p$ to maintain velocity and conductivity. This explains our observations.

Discussion

Saturation degree of pores

We firstly consider the shape of pores in granite rock samples on the basis of the confining pressure dependence of velocities. For simplicity, a pore is supposed to have a spheroidal shape. The closure pressure given by Eq. (1) depends on its aspect ratio and elastic properties of the solid matrix. Since the influence of pores on elastic properties is sufficiently suppressed at high pressures, elastic properties of the solid phase are estimated from velocities in a dry rock sample (AJG02) at 177 MPa (Table 2). The pores closed below 125 MPa must thus have aspect ratios less than 2×10^{-3}. Such oblate spheroidal pores can be treated as circular cracks, and their influence on velocities are formulated in terms of the crack density parameter defined by

$$\varepsilon = \frac{1}{V} \sum a^3 = N_c \langle a^3 \rangle,$$

Table 2 Elastic properties of solid matrix estimated from velocities in dry sample AJG02 at 177 MPa

Properties	Estimated values
Bulk modulus, K	51.9(5) (GPa)
Shear modulus, G	32.3(4) (GPa)
Young's modulus, E	80.3(8) (GPa)
Poisson's ratio, v	0.242(3)

The number inside brackets shows the error in the last digit

where a is the radius of a crack and the summation is over all cracks in a volume V (O'Connell and Budiansky 1974). The crack density parameter is also expressed by the average of a^3 and the number of cracks per unit volume, N_c.

The crack density parameter in a dry sample can be evaluated by comparing measured and calculated velocities. Once the crack density parameter is known, velocities can be calculated for various degrees of fluid saturation (O'Connell and Budiansky 1974). The comparison between measured and calculated velocities will give us an estimation of the saturation degree of pores.

The crack density parameter in Sample AJG04 (wet) was assumed to be identical to that in Sample AJG02 (dry). This assumption should be reasonable since the mean compressional wave velocities in Samples AJG02 and AJG04 were almost identical at atmospheric pressure and dry state (AJG02 4.61(1) km/s, AJG04 4.65(1) km/s). Measured velocities in Sample AJG02 were compared with velocities calculated as a function of the crack density parameter. Elastic properties of the solid phase (Table 2) were used in the calculation of velocity. The crack density parameter at a confining pressure was determined to minimize

$$S = \left(V_p^{\mathrm{obs}} - V_p^{\mathrm{calc}}\right)^2 + \left(V_s^{\mathrm{obs}} - V_s^{\mathrm{calc}}\right)^2.$$

The estimated crack density parameter in Sample AJG02 is shown in Fig. 7 as a function of confining pressure. It rapidly decreases with increasing confining pressure. Measured compressional and shear wave velocities in AJG02 were reasonably reproduced by the estimated crack density parameter (Fig. 8).

The saturation degree in Sample AJG04 (wet) was estimated by comparing measured and calculated velocities. By using the estimated crack density parameter, the compressional and shear wave velocities were calculated as a function of confining pressure for the saturation degrees of 80, 90, and 100 % (Fig. 8). The effect of the fluid is to glue the opposing faces of the crack together with respect to relative normal displacement while not inhibiting relative sliding (O'Connell and Budiansky 1974). In the calculation of
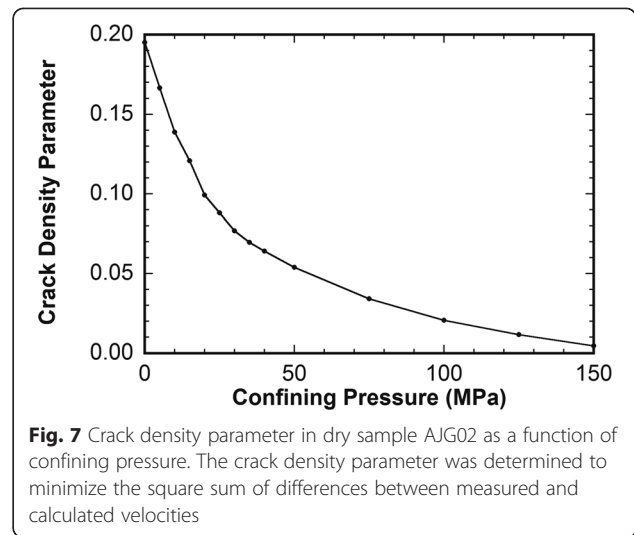

Fig. 7 Crack density parameter in dry sample AJG02 as a function of confining pressure. The crack density parameter was determined to minimize the square sum of differences between measured and calculated velocities
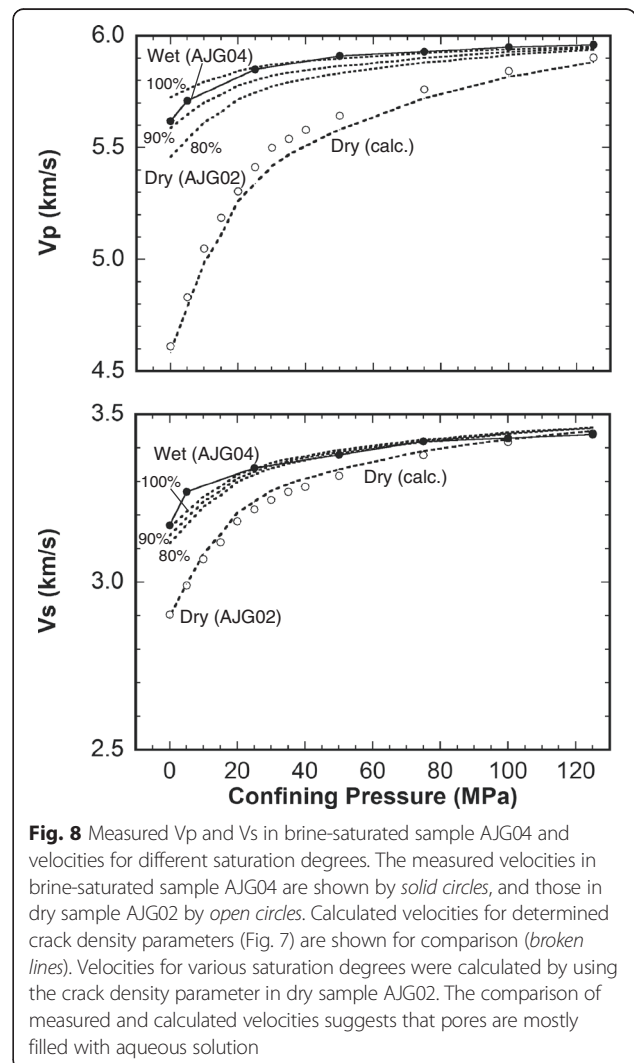

Fig. 8 Measured Vp and Vs in brine-saturated sample AJG04 and velocities for different saturation degrees. The measured velocities in brine-saturated sample AJG04 are shown by *solid circles*, and those in dry sample AJG02 by *open circles*. Calculated velocities for determined crack density parameters (Fig. 7) are shown for comparison (*broken lines*). Velocities for various saturation degrees were calculated by using the crack density parameter in dry sample AJG02. The comparison of measured and calculated velocities suggests that pores are mostly filled with aqueous solution

velocity, all cracks were assumed to be isolated. Even if an elastic wave induces a spatial variation in the fluid pressure, the fluid cannot flow between cracks to reduce the pressure variation. In reality, cracks are interconnected as demonstrated by electrical conductivity. However, the frequency of the elastic wave (2 MHz) is much higher than the characteristic frequency for the flow between cracks,

$$ f = \frac{1}{2\pi} \frac{K}{\eta} \alpha^3 {\sim} 1 \ \ (\text{kHz}), $$

where K, η, and α are the bulk modulus of the solid phase, the viscosity of the fluid, and the aspect ratio of a crack, respectively (O'Connell and Budiansky 1977). Thus, the isolation of cracks is a reasonable assumption. The comparison shows that the degree of saturation must be larger than 90 %. Cracks are then almost completely filled with fluid.

Nature of conduction paths

Conductivity steeply decreases at low pressures and shows small changes at high pressures. Similar changes in conductivity of low-porosity rocks were reported by Brace et al. (1965). Johnson and Manning (1986) devised a percolation model to reasonably reproduce the reported conductivity changes. The percolation model is briefly reviewed, and then it is applied to our results. Based on the comparison between measured and calculated conductivities and microstructural observations, the nature of conduction paths will be discussed.

In the percolation model (Johnson and Manning 1986), the conduction path is modeled as a lattice network with an average coordination number Z and composed of two types of bond: cracks and "pores." Cracks are closed easily with pressure, while "pores" remain open at high pressures. They are randomly distributed on the network. Both cracks and "pores" are assumed to occur as cylindrical tubes with the cross-sectional area of A_c and A_p, which are independent of pressure. The tube length is assumed to be a constant. The occupancy fraction of cracks is denoted by f_c and that of "pores" by f_p. When a crack is closed at a high pressure, it no longer works as a bond. It is treated as a void of the lattice network, and its occupancy fraction is denoted by f_v ($f_c + f_p + f_v = 1$). The effective conductivity, σ_{eff}, of the network is evaluated through the effective medium theory (Kirkpatrick 1973) as

$$ \sum_i f_i \left[\frac{\sigma_{\text{eff}} - \sigma_i}{(Z/2 - 1)\sigma_{\text{eff}} + \sigma_i} \right] = 0, $$

where σ_i is the conductivity of bond i ($i = c, p, v$). The conductivity of bonds is given by

$$ \sigma_i = \frac{\phi_i}{3 f_i} \sigma_f \quad \text{for} \ \ i = c, p $$

$$ \sigma_v = 0, $$

where ϕ_c and ϕ_p are the crack porosity and "pore" porosity, respectively (Johnson and Manning 1986). The fluid conductivity is denoted by σ_f. Because of their stiffness, the occupancy fraction of "pores", f_p, is independent of pressure. Since all cracks are assumed to have the same geometry, the occupancy fraction of cracks, f_c, is proportional to the crack porosity, which is evaluated from strain measurements. The difference between the broken line and the solid curve in Fig. 4 gives the lower bound of the crack porosity as a function of confining pressure.

The conductivity change in Sample AJG04 is compared with the conductivity calculated with the percolation model (Fig. 9). Both calculated and measured values are normalized by the fluid conductivity. The average coordination number Z is set to be 2.3. Johnson and Manning (1986) showed that the steep decrease in conductivity was reasonably well described with an average coordination number slightly greater than 2, and that the calculated values are insensitive to variations of Z in the range $2 < Z < 2.5$. The percolation model roughly reproduces the change in conductivity, though it is a relatively simple model. The steep decrease in conductivity at low pressures is caused by the closure of cracks, which greatly reduces the connectivity of conducting bonds. The conductivity at high pressures is maintained by interconnected stiff "pores."
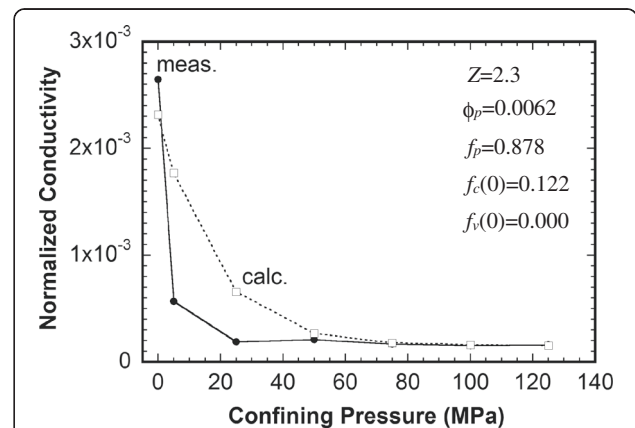

Fig. 9 Measured and calculated conductivities as a function of confining pressure. Conductivities are normalized by the fluid conductivity. The percolation model (Johnson and Manning 1986) was employed for the calculation of conductivity. The crack occupancy fraction is assumed to be proportional to crack porosity. The crack porosity was obtained from the volumetric strain measurement of dry rock sample AJG07

The geometry of cracks should be taken into account for a thorough reproduction of the change in conductivity. Microstructural examination shows that there are three types of pore spaces: intragrain cracks, intergrain cracks (open grain boundaries), and round pores (Fig. 1). Open grain boundaries seem to be the pervasive and the dominant component of the conduction paths at low pressures. In reality, a crack is not an ideal oblate spheroid which closes all at once at a confining pressure. The surface of a crack might be a distribution of asperities which progressively come into contact as the crack closes with pressure (Carlson and Gangi 1985). Wong et al. (1989) measured the crack surface area per unit volume as a function of microcrack aperture and showed that the aperture statistics can be fitted with a power law ($n \sim -1.8$). The crack surface area steeply decreases with its crack aperture. If crack segments have a similar length, segments with smaller apertures close at lower pressures. A power law distribution of aperture thus causes a steep decrease in conductivity at low pressures. On the other hand, crack segments with wide apertures, which are small in area, will be open even at high pressures. The wide segments can work as stiff "pores" and form an interconnected conduction path along with round pores. A quantitative examination of crack aperture should be done on our sample for further understanding.
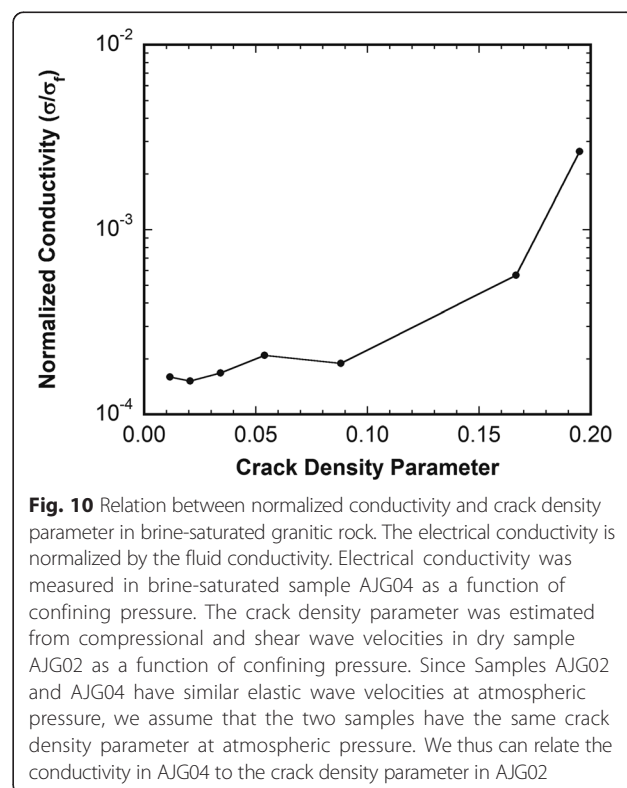
Implication for geophysical observations

Geophysical observations have revealed contrasting variations of seismic velocity and electrical resistivity (the inverse of conductivity) in the continental crust. The variation of seismic velocity is less than 10 % (e.g., Matsubara et al. 2004), while that of resistivity is several orders of magnitude (e.g., Ogawa et al. 2001). The observed resistivity has suggested that aqueous fluids exist pervasively within the crust. The contrasting variations of velocity and conductivity would be explained by the contrasting dependence of velocity and conductivity on the amount of fluid, which was observed in our experiments. We propose a new method for interpreting observed velocity and resistivity.

We at first assume a rock type of a study region and evaluate the crack density parameter from seismic velocity. Seismic velocity in a fluid-saturated rock depends on elastic moduli of the solid and fluid phases and the shape and amount of the fluid phase. When the fluid phase exists within thin cracks, the impact of fluid on effective elastic moduli is formulated with the crack density parameter (O'Connell and Budiansky 1974). When we assume a rock type and give elastic moduli of the solid phase, we can evaluate the crack density parameter to give the observed seismic velocity.

With the obtained crack density parameter, we then evaluate normalized conductivity and evaluate fluid conductivity. Based on our experiments, we now have a relation between the crack density parameter and normalized conductivity (Fig. 10). Electrical conductivity is normalized by the fluid conductivity. The crack density parameter is now limited to the range of 0.01–0.20. For the crack density parameter of 0–0.01, a large increase in the normalized conductivity is expected. The conductivity of dry crustal rocks is estimated to be less than 10^{-4} S/m (e.g., Kariya and Shankland 1983) and that of crustal fluids 10–100 S/m (Nesbitt 1993). The normalized conductivity is thus expected to be less than 10^{-5} at the crack density parameter of zero. There might be an abrupt increase as the crack density increases to 0.01.

Once we have a relation between the crack density parameter and normalized conductivity in the study region, we can evaluate normalized conductivity from the crack density parameter. The inverse of normalized conductivity gives normalized resistivity: the resistivity normalized by the fluid resistivity. Dividing the observed resistivity by the normalized resistivity leads to the fluid resistivity. Its inverse gives the fluid conductivity. If the obtained fluid conductivity is an unrealistic value, we should change the rock type and evaluate the crack density parameter and normalized conductivity. Since the number of parameters to be estimated is larger than

Fig. 10 Relation between normalized conductivity and crack density parameter in brine-saturated granitic rock. The electrical conductivity is normalized by the fluid conductivity. Electrical conductivity was measured in brine-saturated sample AJG04 as a function of confining pressure. The crack density parameter was estimated from compressional and shear wave velocities in dry sample AJG02 as a function of confining pressure. Since Samples AJG02 and AJG04 have similar elastic wave velocities at atmospheric pressure, we assume that the two samples have the same crack density parameter at atmospheric pressure. We thus can relate the conductivity in AJG04 to the crack density parameter in AJG02

that of observables, we will have large uncertainties in the interpretation. The appropriateness of the interpretation should be checked from geological and petrological points of view.

Through the above scheme of interpretation, we can infer rock type, fluid conductivity, and crack density parameter. The estimation of the fluid volume fraction requires the information about the aperture of cracks. If we denote the mean aspect ratio of cracks by α, the fluid volume fraction ϕ is related to the crack density parameter ε as

$$\phi = \frac{4}{3}\pi\alpha\varepsilon.$$

This gives a rough estimate of the fluid volume fraction.

The relation between the crack density parameter and normalized conductivity should be further studied. It is only an empirical relationship, and its applicability to geophysical observations and limitations are not understood. However, as we showed above, once we have such a relation, we can quantitatively interpret seismic velocity and electrical conductivity. The applicability and limitations should be studied both experimentally and theoretically. In experimental studies, the relation between the crack density parameter and normalized conductivity should thus be investigated in a wider range of the crack density parameter in the same rock type. It should also be studied in different rock types. Further theoretical works on the network of grain boundary cracks should give us a basis of the relation between the crack density parameter and normalized conductivity.

Conclusions

Elastic wave velocity and electrical conductivity in a brine-saturated granitic rock were simultaneously measured. Contrasting changes in velocity and conductivity were observed. As the confining pressure increased to 50 MPa, compressional and shear wave velocities increased by less than 10 %. On the other hand, electrical conductivity decreased by an order of magnitude. Both changes must be caused by the closure of cracks under pressures.

Microstructural examinations showed that most cracks were open grain boundaries. In reality, a crack is composed of many segments with different apertures. If crack segments have a similar length, segments with small apertures are closed at low pressures to greatly reduce conductivity, while those with wide apertures are open even at high pressures. The latter must form an interconnected fluid path to maintain the electrical conduction through fluid. A power law distribution of apertures will cause a steep decrease in conductivity at low pressures.

An empirical relation between the crack density parameter and normalized conductivity was obtained. The normalized conductivity is the ratio of bulk conductivity to the conductivity of a pore fluid. This relation should be the basis for a quantitative interpretation of observed seismic velocity and electrical conductivity.

Author details

[1]Graduate School of Science and Engineering, University of Toyama, 3190 Gofuku, Toyama 930-8555, Japan. [2]Now at Yachiyo Engineering Co., Ltd., 1-4-70 Siromi, Chuo-ku, Osaka 540-0001, Japan.

References

Biot MA, Willis DG. The elastic coefficients of the theory of consolidation. J Appl Mech. 1957;24:594–601.

Brace WF, Orange AS, Madden TR. The effect of pressure on the electrical resistivity of water-saturated crystalline rocks. J Geophys Res. 1965;70:5669–78.

Carlson RL, Gangi AF. Effect of cracks on the pressure dependence of P wave velocities in crystalline rocks. J Geophys Res. 1985;90:8675–84.

Christensen NI. Pore pressure and oceanic crustal seismic structure. Geophys J Roy Astron Soc. 1984;79:411–23.

Christensen NI, Wang HF. The influence of pore pressure and confining pressure on dynamic elastic properties of Berea sandstone. Geophys. 1985;50:207–13.

Eshelby J. The determination of the elastic field of an ellipsoidal inclusion, and related problems. Proc R Soc Lond A. 1957;241:376–96.

Geertsma J. The effect of fluid pressure decline on volumetric changes of porous rocks. Petrol Trans AIME. 1957;210:331–40.

Hearmon RFS. The elastic constants of crystals and other anisotropic materials. In: Hellwege KH, Hellwege AM, editors. Landolt-Börnstein Tables, III/11. Berlin: Springer-Verlag; 1979. p. 854.

Johnson DL, Manning HJ. Theory of pressure dependent resistivity in crystalline rocks. J Geophys Res. 1986;91:11611–7.

Kariya KA, Shankland TJ. Electrical conductivity of dry lower crustal rocks. Geophys. 1983;48:52–61.

Kirkpatrick S. Percolation and conduction. Rev Modern Phys. 1973;45:574–88.

Lockner DA, Byerlee JD. Complex resistivity measurements of confined rock. J Geophys Res. 1985;90:7837–47.

Matsubara M, Hirata N, Sato H, Sakai S. Lower crustal fluid distribution in the northeastern Japan arc revealed by high-resolution 3D seismic tomography. Tectonophys. 2004;388:33–45.

Nesbitt BE. Electrical resistivities of crustal fluids. J Geophys Res. 1993;98:4301–10.

O'Connell RJ, Budiansky B. Seismic velocity in dry and saturated cracked solids. J Geophys Res. 1974;79:5412–26.

O'Connell RJ, Budiansky B. Viscoelastic properties of fluid-saturated cracked solids. J Geophys Res. 1977;82:5719–35.

Ogawa Y, Mishina M, Goto T, Satoh H, Oshiman N, Kasaya T, et al. Magnetotelluric imaging of fluids in intraplate earthquake zones, NE Japan back arc. Geophys Res Lett. 2001;28:3741–4.

Rutter EH. Pressure solution in nature, theory and experiment. J Geol Soc Lond. 1983;140:725–40.

Schmeling H. Numerical models on the influence of partial melts on elastic, anelastic and electrical properties of rocks. Part II: electrical conductivity. Phys Earth Planet Inter. 1986;43:123–36.

Sibson R. Rupturing in overpressured crust during compressional inversion—the case from NE Honshu, Japan. Tectonophys. 2009;473:404–16.

Takei Y. Effect of pore geometry on V_P/V_S: from equilibrium geometry to crack. J Geophys Res. 2002. doi:10.1029/2001JB000522.

Walsh JB. The effect of cracks on the compressibility of rock. J Geophys Res. 1965;70:381–9.

Watanabe T, Higuchi A. A new apparatus for measuring elastic wave velocity and electrical conductivity of fluid-saturated rocks at various confining and pore-fluid pressures. Geofluids. 2014;14:372–8.

Watanabe T, Katagishi Y. Deviation of linear relation between streaming potential and pore fluid pressure difference in granular material at relatively high Reynolds numbers. Earth Planets Space. 2006;58:1045–51.

Watanabe T, Shirasugi Y, Yano H, Michibayashi K. Seismic velocity in antigorite-bearing serpentinite mylonites. Geol Soc Lond Spec Pub. 2011;360:97–112.

Wong TF, Fredrich JT, Gwanmesia GD. Crack aperture statistics and pore space fractal geometry of Westerly granite and Rutland quartzite: implications for an elastic contact model of rock compressibility. J Geophys Res. 1989;94:10267–78.